5

Numerical Simulation of Pneumatic and Cyclonic Dryers Using Computational Fluid Dynamics

Tarek J. Jamaleddine and Madhumita B. Ray
Department of Chemical and Biochemical Engineering,
University of Western Ontario, London, Ontario,
Canada

1. Introduction

Drying is inherently a cross and multidisciplinary area because it requires optimal fusion of transport phenomena and materials science and the objective of drying is not only to supply heat and remove moisture from the material but to produce a dehydrated product of specific quality (Mujumdar, 2004)[1]. There are two main modes of drying used in the heat drying or pelletization processes; namely, direct and indirect modes. Each mode of drying has its merits and disadvantages and the choice of dryer design and drying method varies according to the nature of the material to be handled, the final form of the product, and the operating and capital cost of the drying process.

The drying of various materials at different conditions in a wide variety of industrial and technological applications is a necessary step either to obtain products that serve our daily needs or to facilitate and enhance some of the chemical reactions conducted in many engineering processes. Drying processes consume large amounts of energy; any improvement in existing dryer design and reduction in operating cost will be immensely beneficial for the industry.

With the advance in technology and the high demands for large quantities of various industrial products, innovative drying technologies and sophisticated drying equipment are emerging and many of them remain to be in a developmental stage due to the ever increasing presence of new feedstock and wetted industrial products. During the past few decades, considerable efforts have been made to understand some of the chemical and physical changes that occur during the drying operation and to develop new methods for preventing undesirable quality losses. It is estimated that nearly 250 U.S. patents and 80 European patents related to drying are issued each year (Mujumdar, 2004)[1]. Currently, the method of drying does not end at the food processing industry but extends to a broad range of applications in the chemical, biochemical, pharmaceutical, and agricultural sectors. In a paper by Mujumdar and Wu (2008)[2], the authors emphasized on the need for cost effective solutions that can push innovation and creativity in designing drying equipment and showed that a CFD approach can be one of these solutions. The collective effort of their research work along with other researchers in the drying industry using mathematical

modeling for the simulation of the drying mechanism in commercial dryers demonstrated the CFD capabilities and usefulness for the design and understanding of drying equipment.

In a recent paper by Jamaleddine and Ray (2010)[3], the authors presented a comprehensive review on the application of CFD for the design, study, and evaluation of lab-scale and industrial dryers. The use of different numerical methods such as the finite element, finite volume, and finite difference were fully discussed. Numerical models such as the Eulerian-Eulerian and Eulerian-Lagrangian, used for gas–solid multiphase flow systems were also discussed along with their merits, disadvantages, and the scope of their applicability. The application of Kinetic theory approach for granular flow was also discussed. The authors pointed out some of the merits and shortcomings of CFD methods in general, and the drying application, in particular. They argued that a key advantage of CFD methods in evaluating drying systems is that it makes it possible to evaluate geometric changes (different feed point layouts such as multiple entry points) and operating conditions with much less time (faster turnaround time) and expense (flexibility to change design parameters without the expense of hardware changes) than would be involved in laboratory testing. A second advantage is that CFD provides far more detailed output information (suited for trouble-shooting) and far better understanding of the dryer performance than can be obtained in a laboratory environment. By interpreting graphical predictions from a CFD solution, local conditions of all phases in the drying chamber can be evaluated and crucial information related to the dispersion of particulate material can be gathered.

Despite the fact that CFD methods can offer valuable information and a great deal of insight of the process, the use of CFD methods requires considerable expertise. Lack of in-depth knowledge of the CFD methods and insufficient proficiency in utilizing commercial CFD software packages are major concerns for implementing CFD solutions in unknown and unconventional systems. In addition, CFD models have inherent limitations and challenges. Massah et al. (2000)[4] indicated some of the computational challenges of CFD modeling in the drying applications of granular material as follows. First of all, most processes involve solids with irregular shapes and size distribution, which might not be easily captured by some models. Second, Eulerian-Eulerian CFD methods rely on the kinetic theory approach to describe the constituent relations for solids viscosity and pressure, which are based on binary collisions of smooth *spherical* particles and do not account for deviations in shape or size distribution. Finally, very little is known about the turbulent interaction between different phases; thus, CFD models might not have the ability of presenting the associated drag models for a specific case study especially when solids concentration is high. In addition to the above, note that CFD simulations of three-dimensional geometries are computationally demanding and might be costly and although in some cases, the computational effort can be reduced by modeling a two-dimensional representation of the actual geometry (mostly for axisymmetric systems), the realistic behaviour of the simulated system might not be fully captured. Some geometrical systems cannot be modeled using the above simplification and thus, the computational effort becomes a must. This argument also applies to models adopting the Eulerian-Lagrangian formulation for *dense systems* which determine the trajectories of particles as they travel in the computational domain. In addition, formulas describing cohesion and frictional stresses within solids assembly are also not well established in these models. Finally, changes in particle size due to attrition, agglomeration, and sintering are difficult to account for.

As for the heat- and mass-transfer correlations used in commercial CFD packages, very few are provided and the implementation of modified correlations or newly added ones to those already presented or provided by a commercial software demands the need for user defined function subroutines (UDF). This method can become very complicated and usually require many hours of coding and debugging. Although the heat-transfer model capabilities are well improved and capture the heat-transfer mechanism to a reasonable extent, average Nusselt number correlations are used instead of local values. This in turn, reduces the accuracy of the solution results. Additionally, the nature of the CFD equations is approximated which captures the solution results based on approximated assumptions and not on the exact solutions. From a mass-transfer capabilities point of view, mass-transfer models still lack robustness and are hardly included in the current available commercial software. The physics behind these transfer mechanisms is rich and complex, and not entirely captured by CFD methods due to its reliance on experimental observations and correlated equations. Thus, although *qualitative* predictions might be attainable to a reasonable extent, *quantitative* predictions are still the biggest challenge.

2. Numerical models

Multiphase flow models have improved substantially during the past years due to a better understanding of the physical phenomena occurring in multiphase flow systems. An extensive research has also led to a better understanding of the kinetic theory for granular flow and therefore, better implementation of the mathematical formulations pertaining to the flow, heat, and mass transfer mechanisms occurring in multiphase flow systems. The present numerical models for multiphase flows incorporate two approaches: the Eulerian-Eulerian approach, and the Eulerian-Lagrangian approach. A decision on whether the Eulerian-Eulerian or Eulerian-Lagrangian formulation of the governing equations is to be used should be made prior to the numerical solution, simply because each formulation has its limitations and constraints. Numerical predictions obtained from each formulation are not identical, and the choice of a convenient formulation for a specific model relies on whether a dense or dilute system is being considered and the objectives of the numerical study. For instance, if the objective of the numerical model is to follow the trajectories of individual particles, then the Eulerian-Lagrangian formulation appears more convenient for a dilute system (volume fraction of 1% and less). However, for a dense system, this approach is computationally expensive and time consuming and requires powerful and high-speed computers. On the contrary, the Eulerian-Eulerian formulation can handle both dense and dilute systems; however, it cannot predict the local behavior of particles in the flow field.

The theory behind the Eulerian-Eulerian approach is based on the macroscopic balance equations of mass, momentum, and energy for both phases. Eulerian models assume both phases as two interpenetrating continuum (Enwald et al., 1996)[5] and permit the solution of the Navier-Stokes equations with the assumption of incompressibility for both the gas and dispersed phases. The gas phase is the primary or continuous phase while the solid phase is termed as the dispersed phase. Both phases are represented by their volume fractions and are linked through the drag force in the momentum equation as given by Wen and Yu[6] correlation for a dilute system, Ergun[7] correlation for a dense system, and Gidaspow et al.[8], which is a combination of both correlations for transition and fluctuating systems. An averaging technique for the field variables such as the gas and solid velocities, solid volume

fraction, and solid granular temperature is adopted. With this approach, the kinetic theory for granular flow (KTGF) is adopted to describe the interfacial forces between the considered phases and between each of the phases and the boundaries of the computational domain. The KTGF is based on the flow of nonuniform gases primarily presented by Chapman and Cowling (1970)[9]. The model was then further matured through the work of Jenkins and Savage (1983)[10], Lun et al. (1984)[18], Ding and Gidaspow (1990)[11], Gidaspow et al. (1992)[8], and Gidaspow (1994)[12].

On the other hand, Lagrangian models, or discrete particle models, are derived from Newton's law of motion for the dispersed phase. This approach facilitates the ability to compute the trajectory (path) and motion of individual particles. The interactions between the particles are described by either a potential force (soft particle dynamics)[13] or by collision dynamics (hard particle dynamics)[14]. In the Lagrangian approach, the fluid phase is treated separately by solving a set of time averaged Navier-Stokes equations, whereas the dispersed phase is solved by tracking a large number of particles, bubbles, or droplets in the calculated flow field. By computing the temporal development of a sufficiently large sample of particles, ensemble average quantities describing system performance can be evaluated. Furthermore, using the Lagrangian approach, the dispersed phase can exchange mass, momentum, and energy with the fluid phase through a source term added to the conservation equations. These equations also account for the changes in volume fraction of each phase. As each individual particle moves through the flow field, its trajectory, mass, and heat transfer calculations are obtained from a force balance along with an updated local conditions of the continuous phase by solving mass and energy balance equations. Thus, external forces acting on the solid particle such as aerodynamic, gravitational, buoyancy, and contact due to collisions among the particles and between the particles and the domain boundaries, can be calculated simultaneously with the particle motion using local parameters of gas and solids.

Although the form of the Eulerian momentum equation can be derived from its Lagrangian equivalent by averaging over the dispersed phase, each model has its advantages and disadvantages depending on the objective of the study and the type of system used. With this and the above definitions in mind, we now discuss the merits and shortcomings of each formulation.

2.1 Merits and shortcomings of each approach

Some of the advantages and disadvantages of the Eulerian and Lagrangian formulations are discussed in this section. Examples of their use for actual physical systems are also provided to facilitate and enhance our understanding of the subject and to direct the reader to the appropriate formulation for the problem at hand.

For modeling spray dryers, coal and liquid fuel combustion, and particle-laden flows, the Lagrangian description of the governing equations is more suitable because these systems are considered dilute; that is, they are characterized by low concentration of particles with solid volume fractions on the order of 1% or less. It was previously mentioned that this characteristic of particles density allows the tracking of particles trajectories at different locations in the computational domain with less computational effort than the case for a dense system. Predicting the particles trajectories is the main distinctive advantage of the Lagrangian technique over the Eulerian formulation. This in turn provides the opportunity to evaluate interactions between particles, fluids, and boundaries at the microscopic level

using local flow parameters and gas properties, which is difficult to achieve using a continuum or steady-state model. The total number of particles is tractable from a computational point of view and modeling particle–particle and particle–wall interactions can be achieved with a great success. For additional information on the actual form of the conservation equations used in this approach, refer to Strang and Fix[15] and Gallagher[16].

In order to extend the applicability of single phase equations to multiphase flows, the volume fraction of each phase is implemented in the governing equations as was mentioned earlier. In addition, solids viscosities and stresses need to be addressed. The governing equations satisfying single phase flow will not be sufficient for flows where inter-particle interactions are present. These interactions can be in the form of collision between adjacent particles as in the case of a dilute system, or contact between adjacent particles in the case of dense systems. In the former, dispersed phase stresses and viscosities play a crucial role in the overall velocity and concentration distribution in the physical domain. The crucial factor attributed to this random distribution of particles in these systems is the gas phase turbulence. In cases where particles are light and small, turbulence eddies dominate the particles movement and the interstitial gas acts as a buffer that prevents collision between particles. However, in the case of heavy and large diameter particles (150 mm and higher), particle inertia is sufficient to carry them easily through the intervening gas film, and interactions occur by direct collision. Therefore, solids viscosities and stresses cannot be neglected, and the single phase fundamental equations need to be adjusted to account for the secondary phase interaction as shown in the next section.

2.2 Hydrodynamic model equations

In the previous section, it was mentioned that each phase is represented by its volume fraction with respect to the total volume fraction of all phases present in the computational domain. For the sake of simplicity, let us develop these formulations for a binary system of two phases, a gas phase represented by g, and a solid phase represented by s. Accordingly, the mass conservation equation for each phase q, such that q can be a gas= g or solid= s is:

$$\frac{\partial}{\partial t}\left(\rho_q \alpha_q\right) + \nabla \cdot \left(\rho_q \alpha_q \vec{U}_q\right) = \sum_{p=1}^{n} \dot{M}_{pq} \tag{1}$$

where $\dot{M}_{pq}$ (defined later) represents the mass transfer from the pth phase to the qth phase. When $q=g$, $p=s$, $\dot{M}_{pq} = \dot{M}_{sg} = -\dot{M}_{gs}$. Similarly, the momentum balance equations for both phases are:

$$\frac{\partial}{\partial t}\left(\rho_g \alpha_g \vec{U}_g\right) + \nabla \cdot \left(\rho_g \alpha_g \vec{U}_g \vec{U}_g\right) = -\alpha_g \nabla P + \nabla \cdot \overline{\overline{\tau}}_g + \rho_g \alpha_g \vec{g} +$$
$$\vec{\beta}_{gs} + \dot{M}_{sg} \vec{U}_{gs} + \vec{F}_{vm} \tag{2}$$

$$\frac{\partial}{\partial t}\left(\rho_s \alpha_s \vec{U}_s\right) + \nabla \cdot \left(\rho_s \alpha_s \vec{U}_s \vec{U}_s\right) = -\alpha_s \nabla P_s + \nabla \cdot \overline{\overline{\tau}}_s + \rho_s \alpha_s \vec{g} -$$
$$\vec{\beta}_{gs} - \dot{M}_{sg} \vec{U}_{gs} + \vec{F}_{vm} \tag{3}$$

such that $\vec{U}_{gs}$ is the relative velocity between the phases given by $\vec{U}_{gs} = \left(\vec{U}_g - \vec{U}_s \right)$.

In the above equations, $\vec{\beta}_{gs}$ represents the drag force between the phases and is a function of the interphase momentum coefficient K_{gs}, the number of particles in a computational cell N_d, and the drag coefficient C_D such that:

$$
\begin{aligned}
\vec{\beta}_{gs} &= K_{gs} \left(\vec{U}_g - \vec{U}_s \right) \\
&= N_d C_D \frac{1}{2} \rho_g \left(U_g - U_s \right) \left| \vec{U}_g - \vec{U}_s \right| A_{surface} \\
&= \frac{6\alpha_s}{\pi d_s^3} C_D \frac{1}{2} \rho_g \left(U_g - U_s \right) \left| \vec{U}_g - \vec{U}_s \right| \frac{\pi d_s^2}{4} \\
&= \frac{3}{4} C_D \frac{\alpha_s \rho_g}{d_s} \left(U_g - U_s \right) \left| \vec{U}_g - \vec{U}_s \right|
\end{aligned}
\tag{4}
$$

The form of the drag coefficient in Equation (4) can be derived based on the nature of the flow field inside the computational domain. Several correlations have been derived in the literature. A well established correlation that takes into consideration changes in the flow characteristics for multiphase systems is Ossen drag model presented in Skuratovsky et al. (2003)[17] as follows:

$$
\begin{aligned}
C_d &= \frac{64}{\pi \mathrm{Re}_s} \left(1 + \frac{64}{2\pi} \right) && \text{for } \mathrm{Re}_s < 0.01 \\
C_d &= \frac{64}{\pi \mathrm{Re}_s} \left(1 + 10^x \right) && \text{for } 0.01 < \mathrm{Re}_s < 1.5 \\
x &= -0.883 + 0.906 \ln \left(\mathrm{Re}_s \right) - 0.025 \ln^2 \left(\mathrm{Re}_s \right) \\
C_d &= \frac{64}{\pi \mathrm{Re}_s} \left(1 + 0.138 \mathrm{Re}_s^{0.792} \right) && \text{for } 1.5 < \mathrm{Re}_s < 133 \\
\ln C_d &= 2.0351 - 1.66 \ln \mathrm{Re}_s + \ln^2 \mathrm{Re}_s - 0.0306 \ln^3 \mathrm{Re}_s \\
& && \text{for } 40 < \mathrm{Re}_s < 1000
\end{aligned}
\tag{5}
$$

The form of Reynolds number defined in Equation (5) is a function of the gas properties, the relative velocity between the phases, and the solid phase diameter. It is given by:

$$
\mathrm{Re}_s = \frac{\rho_g \left| \vec{U}_g - \vec{U}_s \right| d_s}{\mu_g}
\tag{6}
$$

The virtual-mass force $\vec{F}_{vm}$ in Equations (2) & (3) accounts for the force needed to accelerate the fluid surrounding the solid particle. It is given by:

$$
\vec{F}_{vm} = \alpha_s \rho_g c_{vm} \left(\frac{d\vec{U}_g}{dt} - \frac{d\vec{U}_s}{dt} \right)
\tag{7}
$$

2.3 Complimentary equations – granular kinetic theory equations

When the number of unknowns exceeds the number of formulated equations for a specific case study, complimentary equations are needed for a solution to be possible. For a binary

system adopting the Eulerian formulation such that $q = g$ for gas and s for solid, the volume fraction balance equation representing both phases in the computational domain can then be given as:

$$\sum_{q=1}^{n} \alpha_q = 1 \tag{8}$$

where $\alpha_q = \dfrac{V_q}{V}$

In the case of collision between the particles in the solid phase, the kinetic theory for granular flow based on the work of Gidaspow et al. (1992)[8] dictates that the solid shear viscosity μ_s can be represented by Equation (9) as follows:

$$\mu_s = \frac{10\rho_s d_s \sqrt{\theta_s \pi}}{96\alpha_s \left(1 + e_{ss}\right) g_o} \left[1 + \frac{4}{5}\alpha_s g_o \left(1 + e_{ss}\right)\right]^2 + \frac{4}{5}\alpha_s \rho_s d_s \left(1 + e_{ss}\right) g_o \left(\frac{\theta_s}{\pi}\right)^{\frac{1}{2}} \tag{9}$$

where e_{ss} is a value between *0* and *1* dictating whether the collision between two solid particles is inelastic or perfectly elastic. When two particles collide, and depending on the material property, initial particle velocity, etc, deformation in the particle shape might occur. The resistance of granular particles to compression and expansion is called the solid bulk viscosity μ_b . According to Lun et al. (1984)[18] correlation, it is given by:

$$\mu_b = \frac{4}{3}\alpha_s \rho_s d_s g_o \left(1 + e_{ss}\right) \left(\frac{\theta_s}{\pi}\right)^{\frac{1}{2}} \tag{10}$$

In addition, the solid pressure P_s is given by Gidaspow and Huilin (1998)[19] as:

$$P_s = \alpha_s \rho_s \theta_s \left[1 + 2\left(1 + e_{ss}\right)\alpha_s g_o\right] \tag{11}$$

where θ_s is the granular temperature which measures the kinetic energy fluctuation in the solid phase written in terms of the particle fluctuating velocity c as:

$$\theta_s = c^2 \big/ 3 \tag{12}$$

This parameter can be governed by the following conservation equation:

$$\frac{3}{2}\left[\frac{\partial}{\partial t}\left(\rho_s \alpha_s \theta_s\right) + \nabla \cdot \left(\rho_s \alpha_s \vec{U}_s \theta_s\right)\right]$$
$$= \left(-P_s \overline{\overline{I}} + \overline{\overline{\tau}}_s\right) : \nabla \cdot \vec{U}_s + \nabla \cdot \left(k_s \nabla \theta_s\right) - \gamma_s - 3\beta_{sg}\theta_s \tag{13}$$

where the first term on the right hand side (RHS) is the generation of energy by the solid stress tensor; the second term represents the diffusion of energy; the third term represents the collisional dissipation of energy between the particles; and the fourth term represents the energy exchange (transfer of kinetic energy) between the gas and solid phases.

The diffusion coefficient for the solid phase energy fluctuation given by Gidaspow et al. (1992)[8] is:

$$k_s = \frac{150\rho_s d_s \sqrt{\theta_s \pi}}{384(1+e_{ss})g_o}\left[1+\frac{6}{5}\alpha_s g_o(1+e_{ss})\right]^2 + 2\alpha_s^2 \rho_s d_s g_o(1+e_{ss})\left(\frac{\theta_s}{\pi}\right)^{\frac{1}{2}} \tag{14}$$

The dissipation of energy fluctuation due to particle collision given by Gidaspow et al. (1992)[8] is:

$$\gamma_s = 3\alpha_s^2 \rho_s g_o\left(1-e_{ss}^2\right)\theta_s\left[\frac{4}{d_s}\left(\frac{\theta_s}{\pi}\right)^{\frac{1}{2}} - \nabla \cdot \vec{U}_s\right] \tag{15}$$

The radial distribution function g_o based on Ding and Gidaspow (1990)[11] model is a measure of the probability of particles to collide. For dilute phases, $g_o \rightarrow 1$; for dense phases, $g_o \rightarrow \infty$.

$$g_o = \frac{3}{5}\left[1-\left(\frac{\alpha_s}{\alpha_{s,\max}}\right)^{\frac{1}{3}}\right]^{-1} \tag{16}$$

2.4 Drying model equations – heat and mass transfer

The conservation equation of energy ($q = g, s$) is given by:

$$\frac{\partial}{\partial t}\left(\rho_q \alpha_q H_q\right) + \nabla \cdot \left(\rho_q \alpha_q \vec{U}_q H_q\right) = -\alpha_q \nabla P + \overline{\overline{\tau}}_q : \nabla \vec{U}_q + Q_{pq} + \dot{M}_{pq} H_q \tag{17}$$

By introducing the number density of the dispersed phase (solid in this case), the intensity of heat exchange between the phases is:

$$Q_{sg} = N_d \pi d_s^2 h\left(T_g - T_s\right) = \frac{6\alpha_s}{d_s}h\left(T_g - T_s\right) = \frac{6\alpha_s}{d_s}m_s c_p \frac{dT_s}{dt} \tag{18}$$

Many empirical correlations are available in the literature for the value of the heat- and mass-transfer coefficients. The mostly suitable for pneumatic and cyclone dryers are those given by Baeyens et al. (1995)[20] and De Brandt (1974)[21]. The Chilton and Colburn analogy for heat and mass-transfer are used as follows:

$$Nu_s = 0.15\,\mathrm{Re}_s \tag{19}$$

$$Nu_s = 0.16\,\mathrm{Re}_s^{1.3}\,\mathrm{Pr}^{0.67} \tag{20}$$

$$Sh = 0.15\,\mathrm{Re}_s \tag{21}$$

$$Sh = 0.16\,\mathrm{Re}_s^{1.3}\,Sc^{0.67} \tag{22}$$

where

$$h = \frac{Nu_s k_{cond}}{d_s} \qquad Pr = \frac{c_p \mu_g}{k_{cond}} \qquad Sc = \frac{\mu_g}{\rho_g D_v} \tag{23}$$

The diffusion coefficient D_v defined in the above equations is assumed to be constant.

As the wet feed comes in contact with the hot carrier fluid, heat exchange between the phases occurs. In this stage, mass transfer is considered negligible. When the particle temperature exceeds the vaporization temperature, water vapor evaporates from the surface of the particle. This process is usually short and is governed by convective heat and mass transfer. This initial stage of drying is known as the constant or unhindered drying period (CDP). As drying proceeds, internal moisture within the particle diffuses to the surface to compensate for the moisture loss at that region, and diffusion mass transfer starts to occur. This stage dictates the transfer from the CDP to the second or falling rate drying period (FRP) and is designated by the critical moisture content. This system specific value is crucial in depicting which drying mechanism occurs; thus, it has to be accurate. However, it is not readily available and should be determined from experimental observations for different materials. An alternative approach that bypasses the critical value yet distinguishes the two drying periods is by drawing a comparison to the two drying rates. If the calculated value of diffusive mass transfer is greater than the convective mass transfer, then resistance is said to occur on the external surface of the particle and the CDP dominates. However, if the diffusive mass transfer is lower than the convective counterpart, then resistance occurs in the core of the particle and diffusion mass transfer dominates.

The governing equation for the CDP is expressed in Equation (24). This equation can be used regardless of the method adopted to determine the critical moisture content. In cases when the critical moisture content is known, the FRP can then be expressed as shown in Equation (25) such that $X_{eq} \leq X \leq X_{cr}$. When the critical value is not known, Equation (26) can then be used as shown below. This equation was derived based on Fick's diffusion equation[22] for a spherical particle averaged over an elementary volume.

$$\dot{M}_{CDR} = \frac{k_c M}{d_s} \left(\frac{P_{sat}(T_s)}{RT_s} - X_{H2O} \frac{P}{RT_g} \right) \tag{24}$$

$$\dot{M}_{FDR} = \frac{X - X_{eq}}{X_{cr} - X_{eq}} \dot{M}_{CDR} \tag{25}$$

$$\dot{M}_{Diffusion} = \frac{D_v \rho_s \pi^2}{R^2} \left(\overline{X} - X_{eq} \right) \tag{26}$$

In order to obtain the water vapor distribution in the gas phase, the species transport equation (convection-diffusion equation) is used as shown in Equation (27).

$$\frac{\partial}{\partial t} \left(\rho_g \alpha_g Y_g \right) + \nabla \cdot \left(\rho_g \alpha_g \vec{U}_g Y_g \right) = \nabla \cdot \left(\alpha_g \rho_g D_v \nabla Y_g \right) + \dot{M}_{sg} \tag{27}$$

During the drying process, liquid water is removed and the particle density gradually increases. With the assumption of no shrinkage, the particle density is expressed by:

$$\rho_s = \frac{\rho_{H_2O(l)}\rho_{ds}}{X\left(\rho_{ds} - \rho_{H_2O(l)}\right) + \rho_{H_2O(l)}} \tag{28}$$

2.5 Turbulence model equations

To describe the effects of turbulent fluctuations of velocities and scalar quantities in each phase, the $k - \varepsilon$ multiphase turbulent model can be used for simpler geometries. Advanced turbulence models should be used for cases with swirl and vortex shedding (*RANS*, $k - \omega$). In the context of gas-solid models, three approaches can be applied (FLUENT 6.3 User's guide)[23]: (1) modeling turbulent quantities with the assumption that both phases form a mixture of density ratio close to unity (mixture turbulence model); (2) modeling the effect of the dispersed phase turbulence on the gas phase and vice versa (dispersed turbulence model); or (3) modeling the turbulent quantities in each phase independent of each other (turbulence model for each phase). In many industrial applications, the density of the solid particles is usually larger than that of the fluid surrounding it. Furthermore, modeling the turbulent quantities in each phase is not only complex, but also computationally expensive when large number of particles is present. A more desirable option would then be to model the turbulent effect of each phase on the other by incorporating *source* terms into the conservation equations. This model is highly applicable when there is one primary phase (the gas phase) and the rest are dispersed dilute secondary phases such that the influence of the primary phase turbulence is the dominant factor in the random motion of the secondary phase.

2.5.1 Continuous phase turbulence equations

In the case of multiphase flows, the standard $k - \varepsilon$ model equations are modified to account for the effect of dispersed phase turbulence on the continuous phase as shown below:

$$\frac{\partial}{\partial t}\left(\rho_g\alpha_g k\right) + \nabla \cdot \left(\rho_g\alpha_g \vec{U}_g k\right) = \nabla \cdot \left(\alpha_g \frac{\mu_{t,g}}{\sigma_k}\nabla k_g\right) + \alpha_g G_{k,g} - \alpha_g\rho_g\varepsilon_g + \alpha_g\rho_g\Pi_{k_g} \tag{29}$$

and

$$\frac{\partial}{\partial t}\left(\rho_g\alpha_g\varepsilon_g\right) + \nabla \cdot \left(\rho_g\alpha_g\vec{U}_g\varepsilon_g\right) = \nabla \cdot \left(\alpha_g \frac{\mu_{t,g}}{\sigma_\varepsilon}\nabla\varepsilon_g\right) + \alpha_g\frac{\varepsilon_g}{k_g}\left(C_{1\varepsilon}G_{k,g} - C_{2\varepsilon}\rho_g\varepsilon_g\right)$$
$$+ \alpha_g\rho_g\Pi_{\varepsilon_g} \tag{30}$$

In the above equations, Π_{k_g} and Π_{ε_g} represent the influence of the dispersed phase on the continuous phase and take the following forms:

$$\Pi_{k_g} = \sum_{p=1}^{m}\frac{K_{gs}}{\alpha_g\rho_g}\left(k_{gs} - 2k_g + \vec{U}_{gs} \cdot \vec{U}_{dr}\right) \tag{31}$$

$$\Pi_{\varepsilon_g} = C_{3\varepsilon}\frac{\varepsilon_g}{k_g}\Pi_{k_g} \tag{32}$$

The drift velocity $\vec{U}_{dr}$ is defined in Equation (33). This velocity results from turbulent fluctuations in the volume fraction. When multiplied by the interchange coefficient K_{gs}, it serves as a correction to the momentum exchange term for turbulent flows:

$$\vec{U}_{dr} = -\left(\frac{D_s}{\sigma_{gs}\alpha_s}\nabla\alpha_s - \frac{D_g}{\sigma_{gs}\alpha_g}\nabla\alpha_g \right) \tag{33}$$

such that $D_g = D_s = D_{t,sg}$ for Tchen Theory of multiphase flow (FLUENT 6.3 User's guide)[23]. The generation of turbulence kinetic energy due to the mean velocity gradients $G_{k,g}$ is computed from:

$$G_{k,g} = \mu_{t,g}\left(\nabla \cdot \vec{U}_g + \left(\nabla \cdot \vec{U}_g \right)^T \right) : \nabla\vec{U}_g \tag{34}$$

The turbulent viscosity $\mu_{t,g}$ given in the above equation is written in terms of the turbulent kinetic energy of the gas phase as:

$$\mu_{t,g} = \rho_g C_\mu \frac{k_g^2}{\varepsilon_g} \tag{35}$$

The Reynolds stress tensor defined in Equation (13) for the continuous phase is based on the Boussinesq hypothesis[24] given by:

$$\overline{\overline{\tau}}_g = -\frac{2}{3}\left(\rho_g \alpha_g k_g + \rho_g \alpha_g \mu_{t,g}\nabla \cdot \vec{U}_g \right)\overline{\overline{I}} + \rho_g \alpha_g \mu_{t,g}\left(\nabla \cdot \vec{U}_g + \left(\nabla \cdot \vec{U}_g \right)^T \right) \tag{36}$$

2.5.2 Dispersed phase turbulence equations

Time and length scales that characterize the motion of solids are used to evaluate the dispersion coefficients, the correlation functions, and the turbulent kinetic energy of the particulate phase. The characteristic particle relaxation time connected with inertial effects acting on a particulate phase is defined as:

$$\tau_{F,sg} = \rho_g \alpha_s K_{gs}^{-1}\left(\frac{\rho_s}{\rho_g} + C_V \right) \tag{37}$$

The Lagrangian integral timescale calculated along particle trajectories is defined as:

$$\tau_{t,sg} = \frac{\tau_{t,g}}{\sqrt{\left(1 + C_\beta \xi^2 \right)}} \tag{38}$$

where

$$\xi = \frac{\left| \vec{U}_{sg} \right|\tau_{t,g}}{L_{t,g}} \tag{39}$$

and

$$C_\beta = 1.8 - 1.35 \left(\cos \theta \right)^2 \tag{40}$$

In Equation (40), θ is the angle between the mean particle velocity and the mean relative velocity. The constant term $C_V = 0.5$ is an added mass coefficient (FLUENT 6.3 User's guide)[23].

The length scale of the turbulent eddies defined in Equation (39) is given by:

$$L_{t,g} = \sqrt{\frac{3}{2}} C_\mu \frac{k_g^{3/2}}{\varepsilon_g} \tag{41}$$

The turbulence quantities for the particulate phase include

$$k_s = k_g \left(\frac{b^2 + \eta_{sg}}{1 + \eta_{sg}} \right) \tag{42}$$

$$k_{sg} = 2k_g \left(\frac{b + \eta_{sg}}{1 + \eta_{sg}} \right) \tag{43}$$

$$D_{t,sg} = \frac{1}{3} k_{sg} \tau_{t,sg} \tag{44}$$

such that

$$b = \left(1 + C_V \right) \left(\frac{\rho_s}{\rho_g} + C_V \right)^{-1} \tag{45}$$

$$\eta_{sg} = \frac{\tau_{t,sg}}{\tau_{F,sg}} \tag{46}$$

3. Grid generation

The development of a CFD model involves several tasks that are equally important for a feasible solution to exist with certain accuracy and correctness. A reliable model can only be possible when correct boundary and initial conditions are implemented along with a meaningful description of the physical problem. Thus, the development of a CFD model should involve an accurate definition of the variables to be determined; choice of the mathematical equations and numerical methods, boundary and initial conditions; and applicable empirical correlations. In order to simulate the physical processes occurring in any well defined computational domain, governing and complimentary equations are solved numerically in an iterative scheme to resolve the coupling between the field variables. With the appropriate set of equations, the system can be described in two- and three-dimensional forms conforming to the actual shape of the system. In many cases, it is

desirable to simplify the computational domain to reduce computational time and effort and to prevent divergence problems. For instance, if the model shows some symmetry as in the case of a circular geometry, it can be modeled along the plane of symmetry. However, for a possible CFD solution to exist, the computational domain has to be discretized into cells or elements with nodal points marking the boundaries of each cell and combining the physical domain into one computational entity.

It is a common practice to check and test the quality of the mesh in the model simply because it has a pronounced influence on the accuracy of the numerical simulation and the time taken by a model to achieve convergence. Ultimately, seeking an optimum mesh that enhances the convergence criteria and reduces time and computational effort is recommended. A widely used criterion for an acceptable meshing technique is to maintain the ratio of each of the cell-side length within a set number (x/y, y/z, x/z < 3). In practice, and for most computational applications, local residual errors between consecutive iterations for the dependent variables are investigated. In the case of high residual values, it is then recommended to modify the model input or refine the mesh properties to minimize these errors in order to attain a converged solution.

The choice of meshing technique for a specific problem relies heavily on the geometry of the domain. Most CFD commercial packages utilize a compatible pre-processor for geometry creation and grid generation. For instance, FLUENT utilizes Gambit pre-processor. Two types of technique can be used in Gambit, a uniform distribution of the grid elements, or what can be referred to as structured grid; and a nonuniform distribution, or unstructured grid. For simple geometries that do not involve rounded edges, the trend would be to use structured grid as it would be easier to generate and faster to converge. It should be noted that the number of elements used for grid generation also plays a substantial role in simulation time and solution convergence. The finer the mesh, the longer the computational time, and the tendency for the solution to diverge become higher; nevertheless, the higher the solution accuracy.

Based on the above, one tends to believe that it might be wise to increase the number of elements indefinitely for better accuracy in the numerical predictions on the expense of computational effort. In practice, this is not always needed. The modeller should always bear in mind that an optimum mesh can be attained beyond which, changes in the numerical predictions are negligible.

In the following, two case studies are discussed. In each case, the computational domain is discretized differently according to what seemed to be an adequate mesh for the geometry under consideration.

Case 1

Let us consider a 4-m high vertical pipe for the pneumatic drying of sand particles and another 25-m high vertical pipe for the pneumatic drying of PVC particles. For both cases, the experimental data, physical and material properties were taken from Paixao and Rocha (1998)[25] for sand, and Baeyens et al. (1995)[26] for PVC as shown in Table 1. Both models were meshed and simulated in a three-dimensional configuration as shown in Figures 1 and 2.

In Figure 1, hot gas enters the computational domain vertically upward, fluidizes and dries the particles as they move along the length of the dryer. As the gas meets the particles, particles temperature increases until it reaches the wet bulb temperature at which surface

Particle	Sand	PVC
Diameter (mm)	0.38	0.18
Density (g / cm^3)	2.622	1.116
Specific Heat [J / (kg ^{o}C)]	799.70	980.0
Drying Tube		
Height (m)	4.0	25.0
Internal Diameter (cm)	5.25	125.0
Gas Flow rate, W_g (kg/s)	0.03947	10.52
Solids Flow rate, W_s (kg/s)	0.00474	1.51
Inlet Gas Temperature, T_g (^{o}C)	109.4	126.0
Inlet Solids Temperature, T_s (^{o}C)	39.9	-
Inlet Gas Humidity, Y_g (kg/kg)	0.0469	-
Inlet Moisture Content of Particles, X_s (kg/kg)	0.0468	0.206

Paixao and Rocha (1998)[25]

Table 1. Conditions used in the numerical model simulation
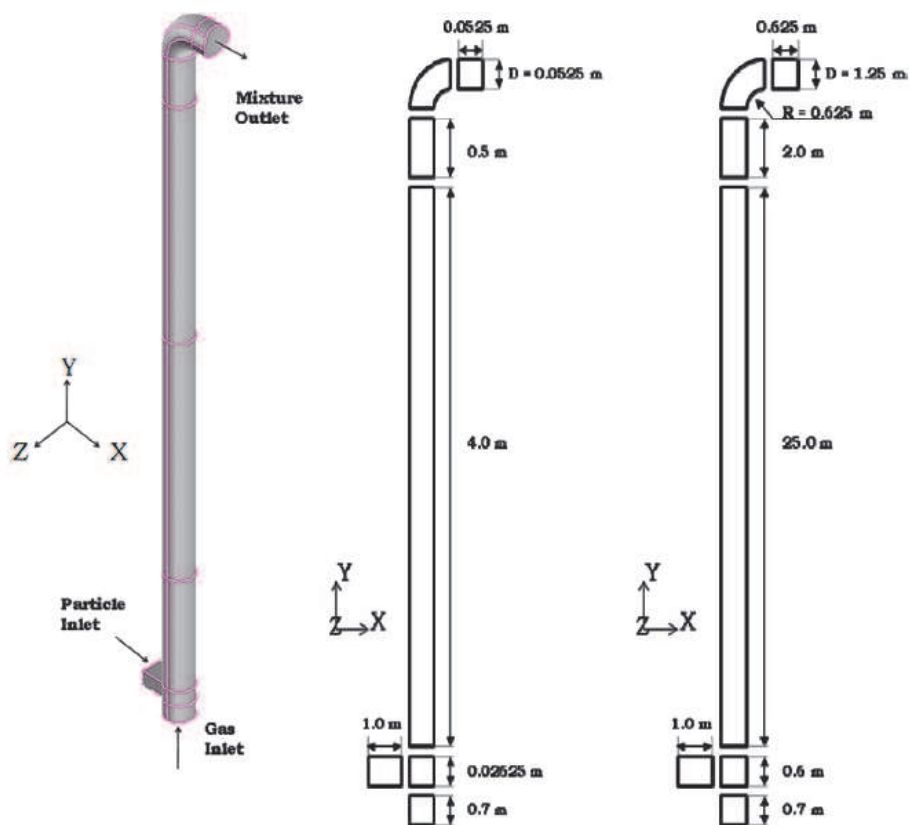
Fig. 1. (Left) Geometrical models; (middle) sand model; (right) PVC model

evaporation starts to occur. At this stage, convective mass transfer dominates the drying of surface moisture of particles during their residence time in the dryer. Since pneumatic drying is characterized by short residence times on the order of 1-10 seconds, mostly convective heat- and mass transfer occur. However, since experimental data for pore moisture evaporation were also provided in the independent literature, moisture diffusion or the second stage of drying was also considered.
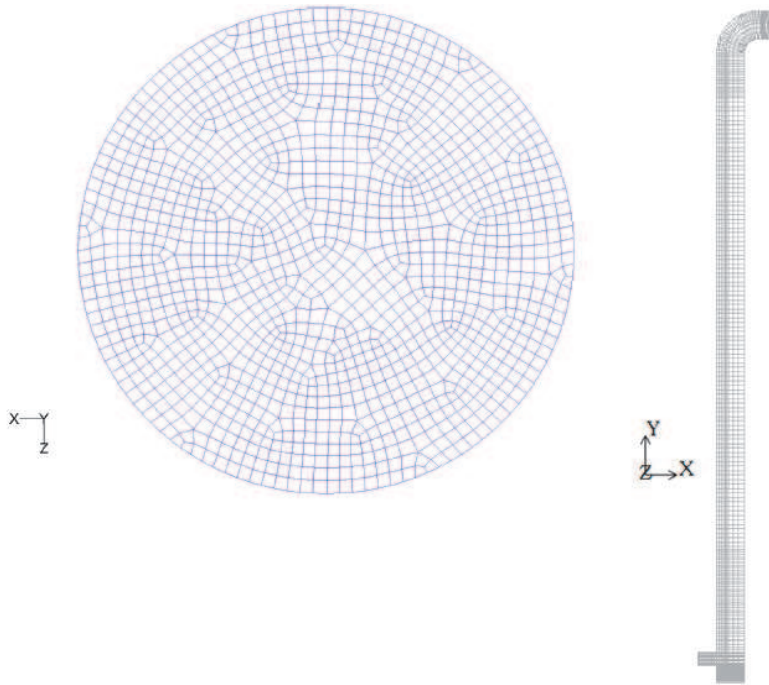

Fig. 2. Computational grid

The computational domain was discretized into hexahedral elements with unstructured mesh in the x and z-directions and nonuniform distribution in the y-direction. An optimized mesh with approximately 63 000 cells and 411 550 cells was applied for the sand and PVC models, respectively. The computational grid is shown in Figure 2. Grid generation was done in Gambit 4.6, a compatible pre-processor for FLUENT 6.3. A grid sensitivity study was performed on the large-scale riser using two types of grids, a coarse mesh with 160 800 elements, and finer mesh with 411 550 elements. All models were meshed based on hexahedral elements due to their superiority over other mesh types when oriented with the direction of the flow. Results obtained for the axial profiles of pressure and relative velocity yield a maximum of 15% difference between the predicted results up to 4.5 m above the dryer inlet; however, there was hardly any difference in the results at a greater length by changing the size of the grids. Therefore, the coarsest grid was used in all simulations.

Case 2

In this case, let us consider a different geometry as shown in Figure 3. This model discusses the drying of sludge material and linked to an earlier work presented by Jamaleddine and

Ray (2010)[3] for the drying of sludge in a large-scale pneumatic dryer. Material properties for sludge are shown in Table 2. The geometrical model is a large-scale model of a design presented by Bunyawanichakul et al. (2006)[28]. The computational domain consists of an inlet pipe, three chambers in the cyclone, and an outlet. Two parallel baffles of conical shape with a hole or orifice at the bottom divide the dryer chambers. As the gas phase and the particulate phase (mixture) enter the cyclone dryer tangentially from the pneumatic dryer, they follow a swirling path as they travel from one chamber to another through the orifice opening. This configuration allows longer residence times for the sludge thus enhancing heat- and mass-transfer characteristics.

Particle	Sludge *
Diameter (mm)	0.18
Density (kg / m³)	998.0
Specific heat [J / (kg ºC)]	4182.0
Thermal Conductivity [W / (m ºC)]	0.6
Drying Tube	
Height (m)	8.0
Internal diameter (m)	6.0

***Sludge properties are taken from Arlabosse et al. (2005) [27]

Table 2. Conditions used in the numerical model simulation

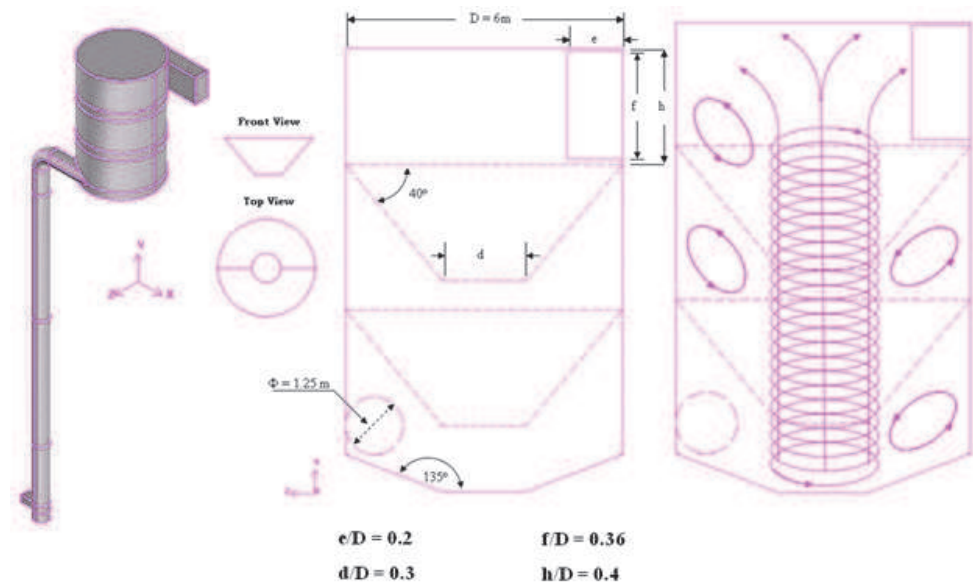e/D = 0.2   f/D = 0.36
d/D = 0.3   h/D = 0.4

Fig. 3. Schematic of the pneumatic-cyclone dryer assembly

The numerical analysis is based on a 3D, Eulerian multiphase CFD model provided by FLUENT/ANSYS R12.0. Physical and material properties for the sludge material are shown in Table 2. The computational domain was discretized into hexahedral elements with approximately 230 385 cells. This element type was chosen as it showed better accuracy between the numerical predictions and experimental data than tetrahedral elements as shown in Bunyawanichakul et al. (2006)[28]. The computational grid is shown in Figure 4. Grid generation was done in Gambit 4.6, a compatible pre-processor for FLUENT.
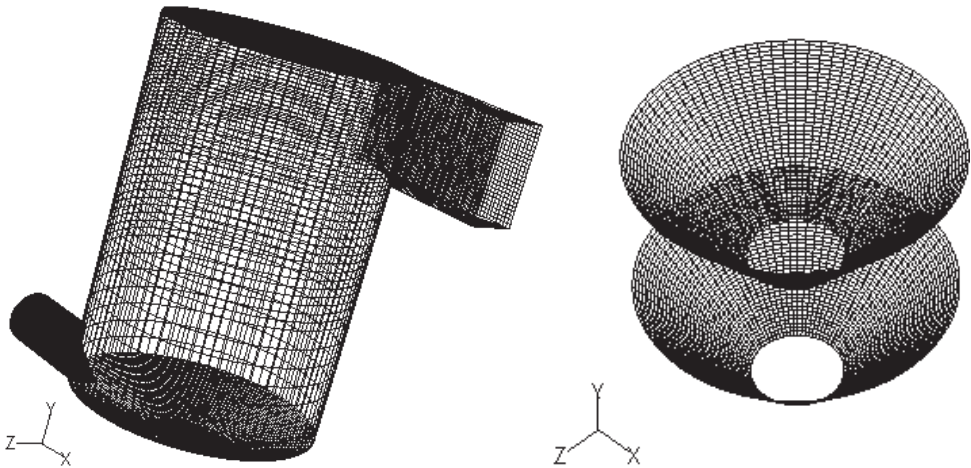
Fig. 4. Computational grid

4. Numerical parameters – numerical solvers

The governing equations along with the complementary equations are solved using a pressure based solution algorithm provided by FLUENT 6.3. This algorithm solves for solution parameters using a segregated method in such a manner that the equations are solved sequentially and in a separate fashion. Briefly stated, the solution parameters are initially updated. The x-, y-, and z-components of velocity are then solved sequentially. The mass conservation is then enforced using the pressure correction equation (SIMPLE algorithm) to ensure consistency and convergence of solution equations. The governing equations are spatially discretized using second-order upwind scheme for greater accuracy and a first-order implicit for time. This allows for the calculation of quantities at cell faces using a Taylor series expansion of the cell-centered solution about the cell centroid. More details related to this can be found in Patankar[29], or FLUENT 6.3 User Guide (2006)[23].

SAND AND PVC MODELS: A modified k-ε turbulence model is used along with the standard wall function for both phases in the vicinity of the wall. To avoid solution divergence, small time steps on the order of 1×10^{-4} to 1×10^{-6} are adopted. Solution convergence is set to occur for cases where scaled residuals for all variables fall below 1×10^{-3}, except for the continuity equation (1×10^{-4}) and the energy equation (1×10^{-6}).

SLUDGE MODEL: For this model, a RNG $k - \varepsilon$ turbulence model is used along with the standard wall function for both phases in the vicinity of the wall. Bunyawanichakul et al.[28] validated their numerical predictions with experimental data by adopting tetrahedral mesh

with Reynolds Stress Turbulence Model (RSTM), and hexahedral mesh with standard and RNG $k - \varepsilon$ turbulence models. It was found that the hexahedral mesh with the RNG $k - \varepsilon$ turbulence model predicted the pressure drop across the dryer chambers as well as the velocity distribution in the chambers reasonably well when used with the second-order advection scheme. In addition, RNG $k - \varepsilon$ turbulence model was successfully applied by Huang et al. (2004)[30,31] for modeling of spray dryers with different designs of atomizer. In order to avoid solution divergence in the current model, small time steps on the order of 1 x 10^{-3} - 1 x 10^{-4} are adopted. Solution convergence is set to occur for cases where scaled residuals far all variables fall below 1 x 10^{-3}, except for the continuity equation (1 x 10^{-4}) and the energy equation 1 x 10^{-6}. The maximum number of iterations per time step is set to 60. It took roughly 40 days for the solution to converge on Windows XP operating system with Core 2 Quad processor.

For all models, User Defined Functions subroutines (UDFs) are introduced to enhance the performance of the code. Accordingly, all UDFs are implemented directly from a source file written in a C programming language subsequently after the case file is read. This feature enables the macro functions to be visible or rather accessible by the user for them to be included in the solution where they should be applied. Equations implemented in UDFs are the following: a) properties pertaining to the drag force between the phases in Equations; b) the radial distribution function; c) the heat transfer coefficient; d) the mass transfer coefficient; and e) the particle density.

5. Results and discussion

In this section, some of the numerical predictions obtained from the CFD simulation for all cases considered in this chapter are shown. For case I, the numerical results agreed well with the experimental data with the following conditions: (i) the turbulent intensity is 5% at
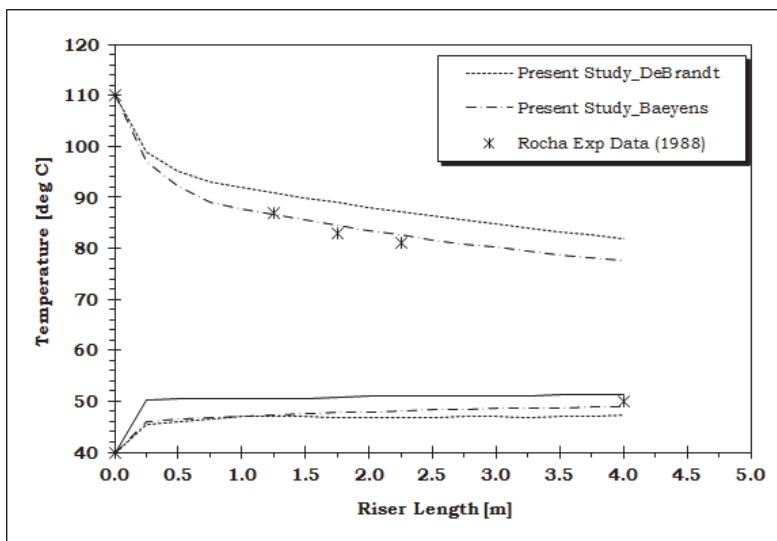

Fig. 5. Prediction of axial gas and particle temperatures along the length of the sand dryer (top lines, gas temperature; bottom lines, particle temperature)

the gas inlet; (ii) the turbulent intensity is 10% at the mixture inlet; (iii) the turbulent viscosity ratio was between 5-10%; (iv) particles were assumed to slip at the wall with specularity coefficient of 0.01; and (v) inelastic particle-wall collision with restitution coefficient of 0.6.
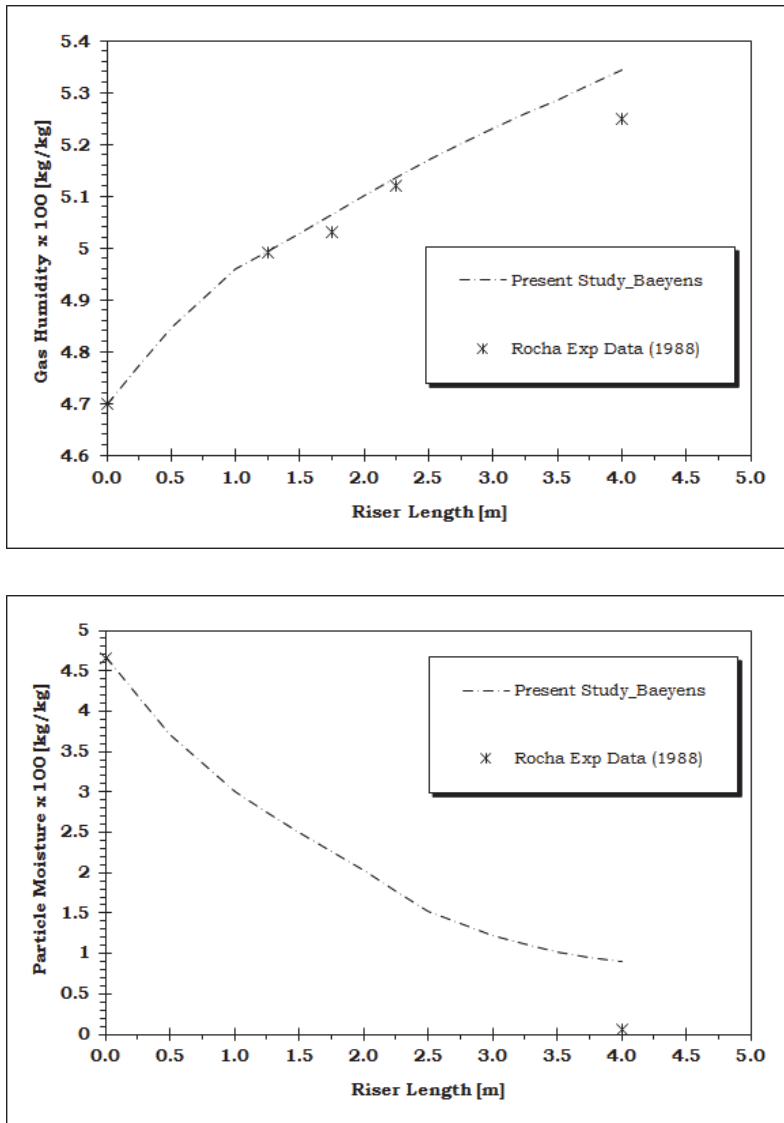

Fig. 6. Prediction of axial gas humidity (top) and particle moisture distribution (bottom) along the length of the sand dryer
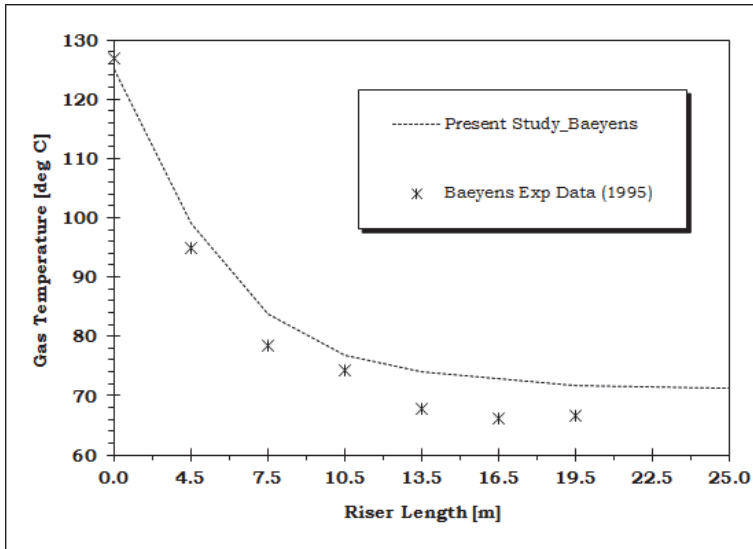
Fig. 7. Prediction of axial gas temperature along the length of the PVC dryer
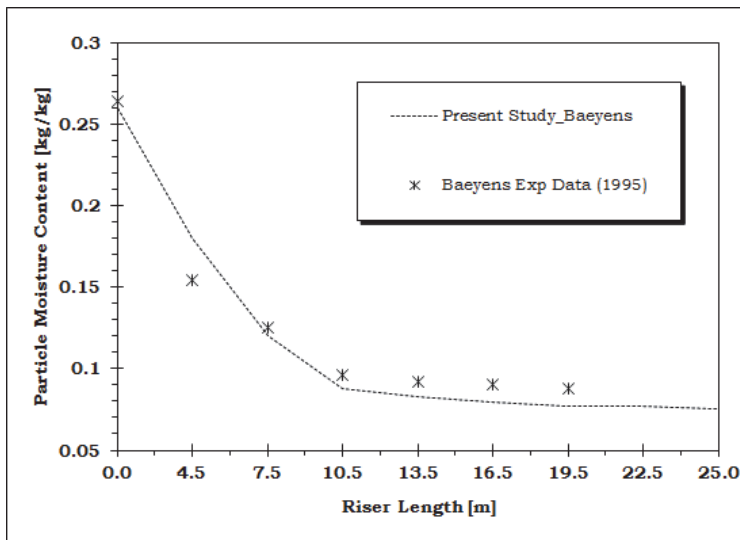

Fig. 8. Prediction of axial particle moisture distribution along the length of the PVC dryer
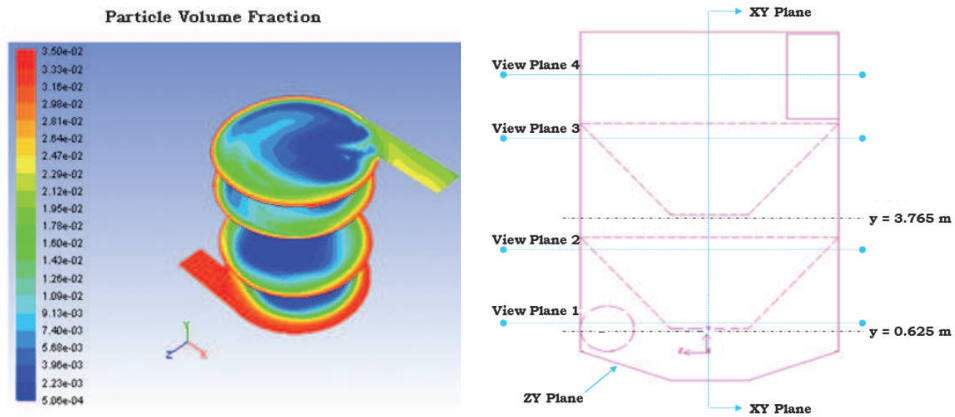
Fig. 9. Contour plot of particulate volume fraction (left) at selected view planes (right)
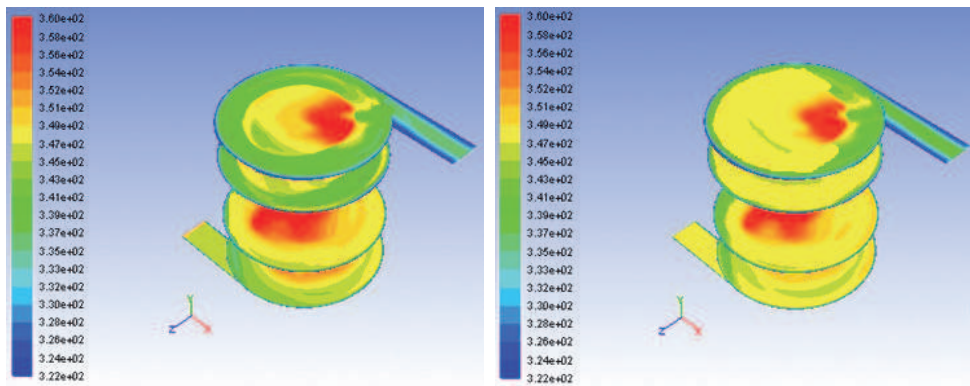

Fig. 10. Contour plot of gas (left) and particle (right) temperatures at selected view planes (Figure 9, right)

For case II, in absence of experimental data we relied more on the qualitative gas and solid velocity patterns in the cyclone dryer. In this case, the UDF capability in FLUENT/ANSYS R12.0 was enhanced by incorporating output data from a pneumatic dryer upstream of the cyclone dryer without facing any divergence or instability issues.

6. Concluding remarks

This chapter demonstrated a simple application of CFD for industrial drying processes. With careful consideration, CFD can be used as a tool to predict the hydrodynamic as well as the heat- and mass-transfer mechanisms occurring in the drying units. It can also be used to better understand and design the drying equipment with less cost and effort than laboratory testing. Although considerable growth in the development and application of CFD in the area of drying is obvious, the numerical predictions are by far still considered as qualitative measures of the drying kinetics and should be validated against experimental results. This is due to the fact that model approximations are used in association with CFD

methods to facilitate and represent complex geometries and reduce computational time and convergence problems.

Although CFD techniques are widely used, the modeller should bear in mind many of the pitfalls that characterize them. Some of these pitfalls are related to but not limited to the choice of the meshing technique; the numerical formulation; the physical correlations; the coding of meaningful and case specific UDFs; the choice from a spectrum of low and high order schemes for the formulation of the governing equations; and last but not least, the choice of iterative and solution dependent parameters.

In addition, due to the complex nature of the processes occurring in the drying systems, extensive simulations must be carried out to demonstrate that the solution is time- and grid-independent, and that the numerical schemes used have high level of accuracy by validating them with either experimental data or parametric and sensitivity analysis. This is particularly crucial in the approximation of the convective terms, as low order schemes are stable but diffusive, whereas high order schemes are more accurate but harder to converge.

7. Nomenclatrue

7.1 General

A	Surface area [m^2]
b	Coefficient in turbulence model [dimensionless]
c	Particle fluctuation velocity [m/s]
$C_{1\varepsilon}, C_{2\varepsilon}, C_{3\varepsilon}$	Turbulence coefficients [=1.42, 1.68, 1.2, respectively]
C_μ	Turbulence coefficient = 0.09 [dimensionless]
c_p	Specific heat capacity of the gas phase [J/kg K]
C_D	Drag coefficient, defined different ways [dimensionless]
c_{vm}	Virtual mass coefficient = 0.5 [dimensionless]
C_g	Vapor concentration in the gas phase [kmol/m^3]
$C_{p,s}$	Vapor concentration at the particle surface [kmol/m^3]
d_s	Particle diameter [m]
D_v	Diffusion Coefficient of water vapor in air [m^2/s]
$D_s, D_{t,sg}$	Turbulent quantities for the dispersed phase
e_{ss}	Particle-particle restitution coefficient [dimensionless]
e_w	Particle-wall restitution coefficient [dimensionless]
F_{vm}	Virtual mass force per unit volume [N/m^3]
$G_{k,g}$	Production of turbulence kinetic energy
g_o	Radial distribution function [dimensionless]
g	Gravitational acceleration constant [m/s^2] ; The gas phase
h	Heat transfer coefficient [W/m^{2}K]
H_{pq}	Interphase enthalpy [J/kg]
H_q	Enthalpy of the q phase [J/kg]
k	Turbulence kinetic energy [m^2/s^2]
K_{Ergun}	Fluid-particle interaction coefficient of the Ergun equation [kg/m^{3}s]
K_{gs}	Interphase momentum exchange coefficient [kg/m^{3}s]
k_{cond}	Thermal conductivity of gas phase [W/m K]
k_c	Convective mass transfer coefficient [m/s]
k_θ	Diffusion coefficient for granular energy

k_g	Turbulence quantity of the gas phase [m²/s²]
k_s	Turbulence quantity of the solid phase [m²/s²]
k_{sg}	Turbulence quantity of the inter-phase [m²/s²]
$L_{t,g}$	Length scale [m]
m_s	Solid mass [kg]
M	Molecular weight [kg/kmol]
$\dot{M}_{pq}$	Mass transfer between phases per unit volume [kg/m³s]
N_d	Number of particles per unit volume [1/m³]
Nu_s	Nusselt number [dimensionless]
P	Pressure [N/m²]
P_s	Solid pressure [N/m²]
P_{sat}	Saturated vapor pressure [Pa]
Pr	Prandtl number [dimensionless]
Q_{pq}	Heat exchange between the phases per unit volume [W/m³]
R	Gas constant [J/kmol K]; Particle radius [m]
Re_s	Solid Reynolds number [dimensionless]
Sc	Schmidt number [dimensionless]
Sh	Sherwood number [dimensionless]
t	Time [s]
T_g	Gas temperature [K]
T_s	Solid temperature [K]
$\vec{U}_q$	Velocity vector of phase q [m/s]
$\vec{U}_g$	Velocity vector of gas phase [m/s]
$\vec{U}_s$	Velocity vector of solid phase [m/s]
$\vec{U}_{sg}$	Relative velocity between the phases [m/s]
$\vec{U}_{dr}$	Drift velocity vector [m/s]
$\vec{U}_{s,\parallel}$	Particle slip-velocity parallel to the wall [m/s]
V	Volume [m³]
X	Particle moisture content [%]
X_{H2O}	Vapor mole fraction in the gas phase [dimensionless]
$\overline{X}$	Mean particle moisture content [%]
Y_q	Mass fraction of vapor in phase q [%]
$\overline{\overline{D}}_q$	Strain-rate tensor for phase q [1/s]

7.2 Greek symbols

α_q	Volume fraction of phase q (s = solid; g = gas)
$\alpha_{s,max}$	Maximum volume fraction of solid phase
β_{sg}	Drag force per unit volume between the phases [N/m³]
γ_s	Collisional dissipation of granular temperature [kg/m³ s]
ε	Turbulent dissipation rate [m²/s³]
ε_g	Turbulent dissipation rate of gas phase [m²/s³]
ε_s	Turbulent dissipation rate of solid phase [m²/s³]

η_{sg}	Turbulence quantity
θ_s	Granular temperature [m²/s²]
θ	Angle [rad]
μ_s	Solid shear viscosity [kg/m s] or [Pa s]
μ_b	Solid bulk viscosity [kg/m s] or [Pa s]
μ_g	Gas dynamic viscosity [kg/m s] or [Pa s]
$\mu_{t,q}$	Turbulence viscosity of phase q [kg/m s] or [Pa s]
K	Inter-phase drag coefficient [kg/m³s]
$\Pi_{k,g}, \Pi_{s,g}$	Influence of dispersed phase on continuous phase
ρ_q	Density of phase q [kg/m³]
ρ_g	Density of the gas phase [kg/m³]
ρ_s	Density of the solid phase [kg/m³]
σ_{gs}	Dispersion Prandtl number = 0.75
σ_k	Turbulent Prandtl number for the turbulent kinetic energy k
σ_ε	Turbulent Prandtl number for the turbulent dissipation rate ε
$\tau_{F,sg}$	Characteristic particle relaxation time connected with inertial effects [s]
$\overline{\overline{\tau}}_s$	Solid stress tensor [N/m²]
$\tau_{t,g}$	Characteristic time of the energetic turbulent eddies [s]
$\tau_{t,sg}$	Lagrangian integral time scale [s]
$\overline{\overline{\tau}}_q$	Reynolds stress tensor [N/m²] or [Pa]
∇	Rate of change in special coordinate [1/m]
$\overline{\overline{I}}$	Identity matrix

7.3 Subscripts

|	
cr	Critical property
ds	Dry solid property
eq	Equilibrium property
g	Gas property
$H2O(l)$	Liquid water
o	Initial condition
q,p	Phase property (s = Solid; g = Gas)
s	Solid property
sat	Saturated condition
vm	Virtual mass

7.4 Superscripts

$\rightarrow$	Vector quantity
$=$	Tensor quantity

8. References

[1] Mujumdar, A.S. Research and development in drying: Recent trends and future prospects. Drying Technology 2004, *22* (1-2), 1 - 26.

[2] Mujumdar, A.S.; Wu, Z. Thermal drying technologies — Cost effective innovation aided by mathematical modeling approach. Drying Technology 2008, *26*, 146 - 154.

[3] Jamaleddine, T.J.; Ray, M.B. Application of computational fluid dynamics for simulation of drying processes: A review. Drying Technology 2010, *28* (2), 120 - 154.

[4] Massah, H.; Oshinowo, L. Advanced gas-solid multiphase flow models offer significant process improvements. Journal Articles by Fluent Software Users 2000, *JA112*, 1 - 6.

[5] Enwald, H.; Peirano, E.; Almstedt, A.E. Eulerian two-phase flow theory applied to fluidization. International Journal of Multiphase Flow 1996, *22* (suppl.), 21 - 66.

[6] Wen, C.Y.; Yu, Y.H. Mechanics of fluidization. Chemical Engineering Progress Symposium Series 1996, *62*, 100 – 111.

[7] Ergun, S. Fluid flow through packed columns. Chemical Engineering Progress 1952, *48*, 89 - 94.

[8] Gidaspow, D.; Bezburuah, R.; Ding, J. Hydrodynamics of circulating fluidized beds, kinetic theory approach. Fluidization VII Proceedings of the 7th Engineering Foundation Conference on Fluidization, Gold Coast, Australia 1992, 75 - 82.

[9] Chapman, S.; Cowling, T.G. *The mathematical theory of non-uniform gases*. 3rd ed., Cambridge University Press: Cambridge, U.K., 1970.

[10] Jenkins, J.T.; Savage, S.B. A theory for the rapid flow of identical, smooth, nearly elastic, spherical particles. J. Fluid Mech. 1983, *130*, 187 - 202.

[11] Ding, J.; Gidaspow, D. A bubbling fluidization model using kinetic theory of granular flow. AIChE J. 1990, *36*(4), 523 - 538.

[12] Gidaspow, D. *Multiphase Flow and Fluidization*. Academic Press, Inc., New York, 1994.

[13] Tsuji, Y.; Kawagushi, T.; Tanaka, T. Discrete particle simulation of two-dimensional fluidized bed. Powder Technology 1993, *77*, 79 - 87.

[14] Hoomans, B.P.B.; Kuipers, J.A.M.; Briels, W.J.; Van Swaaij, W.P.M. Discrete particle simulation of bubble and slug formation in a two-dimensional gas-fluidised bed: A hard-sphere approach. Chemical Engineering Science 1996, 51, 99–118.

[15] Strang, G.; Fix, G. *An Analysis of the Finite Element Method*. Prentice-Hall: Englewood Cliffs, NJ, 1973.

[16] Gallagher, R.H. *Finite Element Analysis: Fundamentals*. Prentice-Hall: Englewood Cliffs, NJ, 1975.

[17] Skuratovsky, I.; Levy, A.; Borde, I. Two-fluid two-dimensional model for pneumatic drying. Drying Technology 2003, *21*(9), 1649 – 1672.

[18] Lun, C.K.K.; Savage, S.B.; Jeffrey, D.J.; Chepurnity, N. Kinetic theories for granular flow: Inelastic particles in couette flow and slightly inelastic particles in a general flow field, J. Fluid Mechanics 1984, 140, 223 - 256.

[19] Gidaspow, D.; Huilin, L. Equation of State and Radial Distribution Function of FCC Particles in a CFB. AIChE J. 1998, 279.

[20] Baeyens, J.; Gauwbergen, D. van; Vinckier, I. Pneumatic drying: the use of large-scale experimental data in a design procedure. Powder Technology 1995, *83*, 139 – 148.

[21] De Brandt, IEC Proc. Des. Dev. 1974, *13*, 396.

[22] Fick, A. *Ueber Diffusion*. Poggendorff's Annals of Physics 1855, *94*, 59 - 86.

[23] FLUENT 6.3 User's Guide. Fluent Incorporated, Lebanon, NH, 2006.

[24] Hinze, J. O. *Turbulence*. McGraw-Hill Publishing Co., New York, 1975.

[25] Paixãˉo, A.E.A.; Rocha, S.C.S. Pneumatic drying in diluted phase: Parametric analysis of tube diameter and mean particle diameter. Drying Technology 1998, *16* (9), 1957 - 1970.

[26] Baeyens, J.; van Gauwbergen, D.; Vinckier, I. Pneumatic drying: The use of large-scale experimental data in a design procedure. Powder Technology 1995, *83*, 139 - 148.

[27] Arlabosse, P.; Chavez, S.; Prevot, C. Drying of municipal sewage sludge: From a Laboratory scale batch indirect dryer to the paddle dryer. Brazilian Journal of Chemical Engineering 2005, *22*, 227 - 232.

[28] Bunyawanichakul, P.; Kirkpatrick, M.; Sargison, J.E.; Walker, G.J. Numerical and experimental studies of the flow field in a cyclone dryer. Transactions of the ASME 2006, *128*, 1240 - 1250.

[29] Patankar, S.V. *Numerical Heat Transfer and Fluid Flow*. McGraw-Hill, New York, 1980.

[30] Huang, L.X.; Kumar, K.; Mujumdar, A.S. Simulation of a spray dryer fitted with a rotary disk atomizer using a three-dimensional computational fluid dynamic model. Drying Technology 2004, *22*(6), 1489 - 1515.

[31] Huang, L. X.; Kumar, K.; Mujumdar, A.S. A comparative study of a spray dryer with rotary disc atomizer and pressure nozzle using computational fluid dynamic simulations. Chemical Engineering and Processing 2006, *45*, 461 - 470.
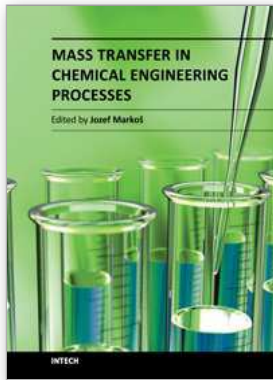
Mass Transfer in Chemical Engineering Processes

Edited by Dr. Jozef Markoš

This book offers several solutions or approaches in solving mass transfer problems for different practical chemical engineering applications: measurements of the diffusion coefficients, estimation of the mass transfer coefficients, mass transfer limitation in separation processes like drying, extractions, absorption, membrane processes, mass transfer in the microbial fuel cell design, and problems of the mass transfer coupled with the heterogeneous combustion. I believe this book can provide its readers with interesting ideas and inspirations or direct solutions of their particular problems.

How to reference

In order to correctly reference this scholarly work, feel free to copy and paste the following:

Tarek J. Jamaleddine and Madhumita B. Ray (2011). Numerical Simulation of Pneumatic and Cyclonic Dryers Using Computational Fluid Dynamics, Mass Transfer in Chemical Engineering Processes, Dr. Jozef Markoš (Ed.), ISBN: 978-953-307-619-5, InTech, Available from: http://www.intechopen.com/books/mass-transfer-in-chemical-engineering-processes/numerical-simulation-of-pneumatic-and-cyclonic-dryers-using-computational-fluid-dynamics

INTECH
open science | open minds